Journal of Materials Chemistry B

PAPER

View Article Online
View Journal

Cite this: DOI: 10.1039/c4tb01429d

Self-assembled targeting of cancer cells by iron(III)-doped, silica nanoparticles

K. K. Pohaku Mitchell,[a] S. Sandoval,[b] M. J. Cortes-Mateos,[c] J. G. Alfaro,[d] A. C. Kummel[a] and W. C. Trogler*[a]

Received 29th August 2014
Accepted 10th October 2014

DOI: 10.1039/c4tb01429d

www.rsc.org/MaterialsB

Iron(III)-doped silica nanoshells are shown to possess an *in vitro* cell-receptor mediated targeting functionality for endocytosis. Compared to plain silica nanoparticles, iron enriched ones are shown to be target-specific, a property that makes them potentially better vehicles for applications, such as drug delivery and tumor imaging, by making them more selective and thereby reducing the nanoparticle dose. Iron(III) in the nanoshells can interact with endogenous transferrin, a serum protein found in mammalian cell culture media, which subsequently promotes transport of the nanoshells into cells by the transferrin receptor-mediated endocytosis pathway. The enhanced uptake of the iron(III)-doped nanoshells relative to undoped silica nanoshells by a transferrin receptor-mediated pathway was established using fluorescence and confocal microscopy in an epithelial breast cancer cell line. This process was also confirmed using fluorescence activated cell sorting (FACS) measurements that show competitive blocking of nanoparticle uptake by added holo-transferrin.

Introduction

Nanoparticles are being investigated for a variety of biomedical applications including imaging, gene transfer, immune system activation, and targeted drug delivery.[1–12] Active targeting, a method commonly employed in drug delivery applications, requires conjugation of a targeting moiety to the surface of delivery vehicles, such as nanoparticles.[13–15] Compounds that have been investigated as targeting ligands include antibodies, polymers, aptamers, peptides, and proteins.[13,16–19] Addition of a targeting ligand to the surface of a nanoparticle imparts it with specificity for a particular type of cell surface receptor;[20–28] however, conjugation of a targeting ligand can also change nanoparticle properties, such as increasing size or decreasing stability.[13,16,29–33] It also may interfere with other desired surface functionalization. Thus, developing a nanoparticle with a targeting component built into its structure would increase the nanoparticle's versatility.

There is interest in developing nanoparticles that bind the cell-surface transferrin receptor (TfR) overexpressed in cancer cells.[30,34–45] Transferrin (Tf) is a glycoprotein found in serum and is responsible for the transport of iron, which is often a limiting nutrient, to cells. Iron-containing transferrin, known as holo-transferrin (holoTf), is taken into the cell by a transferrin receptor-mediated pathway.[39,46,47] Nanoparticles that target the transferrin receptor are therefore likely to be undergo receptor-mediated endocytosis. Current approaches to TfR-mediated endocytosis first conjugate holo-transferrin to a nanoparticle surface.[30,39,44,48–61] Our work explores the use of iron(III) enrichment of a sol–gel silica nanoparticle to achieve a similar effect.

Incorporation of ~6% iron(III) into the matrix of silica nanoshells was recently shown to impart the resulting nanoshell with biodegradable characteristics.[62] This relied on the well-known ability of living systems to extract iron from their environment.[63–66] It was shown that iron-doped nanoshells dissolved when iron(III) was removed either by small molecule chelation or by biochelating agents in fetal bovine or human serum. It was postulated that iron(III) binding proteins, such as serum transferrin,[65] were responsible for the removal of iron(III) and thus the breakdown of the nanoshell structure. Since iron loss from the doped nanoshells takes several weeks, it seemed likely that during the iron(III) extraction process transferrin could bind to the nanoparticle surface areas with exposed iron(III). This suggested that the incorporation of iron(III) into the silica nanoshell may also impart self-assembled targeting (*i.e.* does not require the covalent conjugation of a targeting moiety to the surface of the nanoshell before use) capabilities that could be used to selectively target TfR rich cells, such as cancer cells.

A variety of cancer cells have been shown to overexpress the transferrin receptor on their surface.[67] Metastatic cancer cell lines, such as the MDA-MB-231 epithelial breast cancer cell line, tend to have greater overexpression of the TfR than the less metastatic members of the same cell line.[68,69] This

[a]University of California San Diego, Dept. of Chemistry and Biochemistry, Mail Code 0358, La Jolla, CA 92093, USA. E-mail: wtrogler@ucsd.edu
[b]University of California San Diego, Dept. of Bioengineering, La Jolla, CA 92093, USA
[c]University of California San Diego, Moores Cancer Center, La Jolla, CA 92093, USA
[d]University of California San Diego, Dept. of Chemical Engineering, La Jolla, CA 92093, USA

overexpression of transferrin receptors by metastatic cancer cells ensures that they receive the iron required to support an increased rate of cellular division. It also provides a receptor for targeting such cancer cells by drug therapies.

This study examines whether the doping of iron(III) into the matrix of silica nanoshells leads to increased uptake, relative to undoped silica nanoshells, by MDA-MB-231 breast cancer cells. The proposed mechanism for enhanced uptake by a transferrin receptor-mediated pathway was tested by blocking the transferrin receptor with varying concentrations of holo-transferrin before addition of nanoshells to the cells. Nanoshell uptake was assessed using fluorescence microscopy or confocal laser scanning microscopy, and blocking was quantified by fluorescence activated cell sorting (FACS).

Experimental

Materials

3-Aminopropyltriethoxysilane (APTES) was obtained from Thermo Fisher Scientific (Carlsbad, CA). Absolute ethanol was purchased from Sigma-Aldrich (St. Louis, MO). Nunc Lab-Tek II 4-well chamber slides were obtained from Fisher Scientific (Pittsburgh, PA). MDA-MB-231 epithelial breast cancer cells were purchased from ATCC (Manassas, VA). Dulbecco's Phosphate Buffered Saline solution without $CaCl_2$ and $MgCl_2$ (DPBS 1×), Dulbecco's Modified Eagle's Medium (DMEM), and fetal bovine serum (FBS) were purchased from Mediatech, Inc. (Manassas, VA). The bovine holo-transferrin was purchased from MP Biomedicals, LLC (Solon, OH). Hoechst 33342 (Eugene, OR), AlexaFluor 680 carboxylate, AlexaFluor 488 carboxylate, chloromethylfluorescein diacetate (CMFDA) CellTrackerTM Green intracellular stain, and Prolong Gold were obtained from Life Technologies (Carlsbad, CA). Paraformaldehyde (PFA) was purchased from Thermo Fisher Scientific (Fair Lawn, NJ). All materials were used as received.

Surface functionalization of nanoshells

Calcined, 100 nm silica and Fe-doped nanoshells were prepared using a sol–gel template growth procedure as described previously.[62] Nanoshell surfaces were modified, using the following procedure. In order to attach a fluorescent dye (either AlexaFluor 488 or AlexaFluor 680), first 5 mg of nanoshells were added to a 15 mL centrifuge tube containing 5 mL of absolute ethanol. A solution of 1% (w/w with respect to the mass of nanoshells) APTES was added to the tube and the mixture was vortex mixed for one hour. The particles were collected *via* centrifugation and washed once with absolute ethanol. After 5 mL of fresh ethanol was added to the particles, the pellet was resuspended, by sonication for 20 min. After sonication, 0.1% (w/w relative to mass of nanoshells) of the desired fluorescent dye was added and the mixture was vortex mixed for 3 h. The fluorescently labeled nanoshells were then centrifuged and the solid washed three times with ethanol and resuspended in 1 mL of MilliQ water by sonication.

Cell culture experiments

MDA-MB-231 epithelial breast cancer cells were grown at 50 000 cells per well on Nunc Lab-Tek II 4-well chamber slides in DMEM supplemented with 10% FBS, 1% antibiotics (penicillin, streptomycin, glutamine) and 1% sodium pyruvate, at 37 °C in a humidified atmosphere of 5% CO_2. Before initiating cell adhesion, endocytosis, or transferrin receptor blocking experiments, the cells were grown to 60–80% well confluence.

Cell adhesion/endocytosis experiments

This method was adapted from a published procedure by Yang *et al.*[70] All concentrations mentioned are added so the total volume in each well was 1 mL, unless stated otherwise. MDA-MB-231 cells were incubated with 50, 100, and 200 μg mL^{-1} of 100 nm, AlexaFluor 680 functionalized, plain SiO_2 and corresponding Fe(III)-doped, SiO_2 nanoshells for 24 h in DMEM complete media at 37 °C in a humidified atmosphere of 5% CO_2. After incubation, the cells are washed twice with DPBS and labeled with 1 μM CMFDA and 0.01 μg mL^{-1} Hoechst in DPBS for 30 min. The cells were subsequently washed twice with DPBS to remove any excess dye. After washing, the cells were fixed by incubating them in 4% PFA in DPBS solution for 15 min. The cells were washed once with DPBS, and then Prolong Gold was added to prepare the slides for visualization by fluorescence and confocal microscopy.

Transferrin receptor (TfR) blocking experiment

MDA-MB-231 cells were incubated with 500 μL of 0, 20, 200, 500, and 1000 μM bovine holo-Tf for 2 h in DMEM complete media at 37 °C in a humidified atmosphere of 5% CO_2. 100 μg mL^{-1} of 100 nm Fe(III)-doped, SiO_2 nanoshells was added to the cells and incubated for 24 h at 37 °C in a humidified atmosphere of 5% CO_2. After the 24 h incubation, the cells were prepared for visualization using fluorescence microscopy by the procedure used for the adhesion/endocytosis experiment.

Fluorescence microscopy of nanoshell uptake by MDA-MB-231 cells

Fluorescence microscopy was used to visualize the uptake of AlexaFluor 680 functionalized, 100 nm plain SiO_2 and Fe(III)-doped, SiO_2 nanoshells in the adhesion/endocytosis and the TfR blocking experiments. Three images (one image for blue Hoechst fluorescence, one for green CMFDA fluorescence, and one for red AlexaFluor 680 fluorescence) were recorded using a Zeiss AxioImager Z1 fluorescence microscope and a 1.4 megapixel Photometrics Cool-SNAP HQ^2 camera. The samples were imaged at 40× magnification and had an image resolution of 0.1566 μm per pixel. The green fluorescence was visualized using a Zeiss 38HE filter set. Zeiss filter sets 49 and 32 were used to visualize the blue and red fluorescence, respectively. The resulting images were compiled and processed using Image J software (NIH, Bethesda, MD). The excitation source was a short arc mercury lamp.

Confocal microscopy of nanoshell uptake by MDA-MB-231 cells

Confocal microscopy was used to visualize the uptake of AlexaFluor 680 modified, 100 nm plain SiO_2 and Fe(III)-doped, SiO_2 nanoshells. Images were captured using a Zeiss LSM510 laser scanning microscope using a 63× objective. Sequential 202 μm × 202 μm (frame size 1024 × 1024) sections were acquired at 1 micron intervals in the z direction at excitation wavelengths of 364, 488, and 633 nm.

Fluorescence activated cell sorting (FACS) to measure TfR blocking

100 000 cells per well were plated in a standard 96-well plate. The cells were centrifuged for 3 min at 2000 rpm and 4 °C and washed with FACS buffer (5% FBS in DPBS) two times. After the washes, 50 μL of DMEM complete was added and the cells were resuspended. Aliquots of 0, 20, 200, 500, and 1000 μM bovine holo-Tf were then added to the respective wells and the cells were incubated for 2 h at 37 °C in a humidified atmosphere of 5% CO_2. The cells were agitated every 20 min during incubation to prevent their adherence to the well. After the 2 h incubation in holo-Tf, 50 μg mL^{-1} (based on a final volume of 100 μL) of AlexaFluor 488 labeled, 100 nm Fe(III)-doped, SiO_2 nanoshells were added and the cells were incubated for another 3 h with agitation in 20 min intervals. The cells were isolated by centrifugation and washed with FACS buffer three times. After the last wash, the supernatant was removed and 100 μL of FACS-fix (4% PFA in DPBS) added and used to resuspend the cells. Once the cells were resuspended, the contents of each well were transferred to the corresponding FACS tube containing 200 μL of FACS-fix. The samples were analyzed and processed using a BD FACSCalibur flow cytometry system and FloJo software (v. 7.6.1), respectively.

Results and discussion

Cell adhesion/endocytosis of 100 nm plain and Fe(III)-doped, SiO_2 nanoshells

Both 100 nm plain and Fe(III)-doped, silica nanoshells were prepared and characterized using previously reported methods.[5,62,71] An SEM image of the calcined Fe(III)-doped nanoshells can be seen in Fig. 1.

Calcined nanoshells were then amine-modified with 3-aminopropyltriethoxysilane so AlexaFluor 680 carboxylate, a fluorescent far red dye, could be covalently linked to the surface of both the plain silica and Fe(III)-doped, silica nanoshells. The procedure for the conjugation of the dye to the nanoshell is given in the Experimental.

The cell adhesion/endocytosis experimental procedure was adapted from a procedure by Yang *et al.*[70] MDA-MB-231 cells were plated in a chamber slide in duplicate. The cells were incubated with 50, 100, and 200 μg mL^{-1} of 100 nm AlexaFluor 680 functionalized, plain SiO_2 or Fe(III)-doped, SiO_2 nanoshells for 24 h in DMEM complete media at 37 °C in a humidified atmosphere of 5% CO_2. After the 24 h incubation, the cells were washed and stained with CMFDA-green, a dye that freely passes

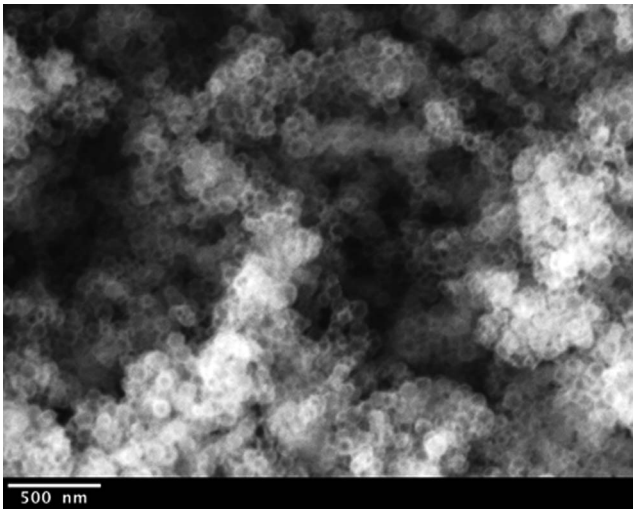

Fig. 1 Scanning electron microscopy image of 100 nm Fe(III)-doped nanoshells before dispersion. The image shows the morphology of the nanoshells. The scale bar in the lower left is 500 nm.

the cell membrane and in the cytoplasm is converted into an impermeable fluorescent product, and Hoechst, a blue fluorescent nucleus stain. Three fluorescence microscopy images (blue, green, and red images) were then captured and the images superimposed and analyzed using Image J as described above. Outlines for the cells were also obtained using Image J and were based on the individual CMFDA green, cytoplasmic stain images.

Fig. 2 shows the fluorescence microscopy images obtained for MDA-MB-231 cells incubated with (a) 0, (b) 50, (c) 100, and (d) 200 μg mL^{-1} of 100 nm plain silica nanoshells and (e) 0, (f) 50, (g) 100, and (h) 200 μg mL^{-1} of 100 nm iron(III)-doped, silica nanoshells. Since the plain and Fe(III)-doped, silica nanoshells are labeled with a red dye, endocytosis of the nanoshells is indicated by the presence of yellow, orange, or red spots within the green boundary of the cell. Panels b–c in Fig. 2 do not exhibit a noticeable difference in cellular uptake of the plain silica nanoshells despite the increase in nanoshell concentration. A few yellow regions can be observed in the panels indicating that a small amount of plain silica nanoshells are taken up by the cells. Given that plain silica nanoshells are only 100 nm in size, it is likely that some are assimilated slowly because of their small size rather than their chemical composition, as endocytosis of small nanoparticles may also occur by non-receptor mediated pathways.[72–74]

The effects of iron(III)-doping into the silica matrix of the nanoshell are evident in Fig. 2, panels f–g. As the concentration of Fe(III)-doped, silica nanoshells increases across panels f–h the amount of cellular adhesion/endocytosis increases as well. The increase in adhesion/endocytosis with increased nanoshell concentration suggests that the doped nanoshells are targeting an iron-uptake pathway in the cells. It has also been shown that silica particles can undergo trans- or exocytosis, so it is possible that iron also aids in intracellular retention due to the availability of local resources.[75] The difference in uptake is

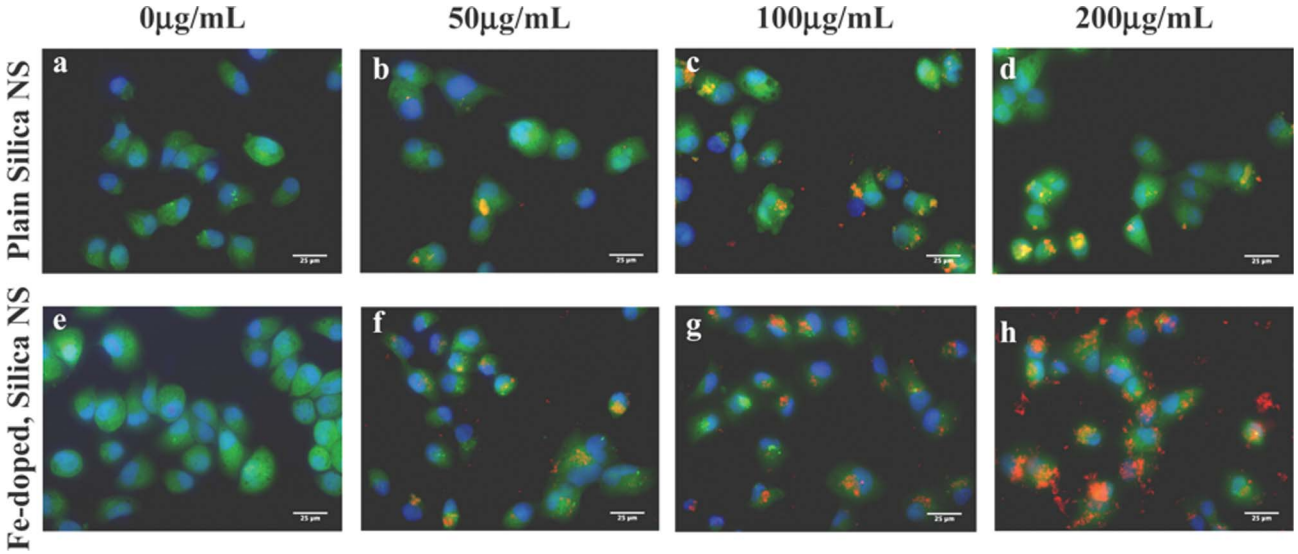

Fig. 2 Fluorescence microscopy images of a cell adhesion/endocytosis experiment with MDA-MB-231 epithelial breast cancer cells. The top row of images (a–d) show that 100 nm plain silica nanoshells are only minimally taken up by the cells regardless of the nanoshell concentration. Images e–h show that as the concentration of iron(III)-doped, silica nanoshells is increased, cellular uptake increases. The scale bar in the lower right corner of all images is 25 microns.

quantified from the images using a previously reported luminescence ratio analysis method.[70] The results of the ratio analysis are provided in Table 1.

As seen in Table 1, the addition of 200 μg nanoshells to the cells does not yield statistically significant differences in the uptake of Fe-doped, SiO_2 nanoshells relative to the plain SiO_2 nanoshells, although the images suggest visually that the iron(III)-doped nanoshell set has more nanoshells interacting with the cells as the concentration was increased. This indicates that cells are being saturated with nanoshells at high concentrations. Thus, the nanoshells may be adhering to the cell or being taken up by a pathway other than the TfR receptor-mediated endocytosis. If one focuses on the two lower concentrations (50 and 100 μg mL^{-1}) of nanoshells, the MDA-MD-231 cells uptake four times more Fe(III)-doped, SiO_2 nanoshells than plain silica nanoshells by mass. It should be noted that the mass of the pure silica nanoshells is roughly half that of the iron doped nanoshells,[76] so the preference on a per particle basis is approximately 8×.

This supports what is seen in the images in Fig. 2. In addition, the image quantification data suggests that using a lower concentration (*i.e.* 50 or 100 μg mL^{-1}) of nanoshells rather than a large saturating dose (for instance, 200 μg mL^{-1} or more) can minimize non-specific nanoshell adhesion/endocytosis. This would imply that less nanomaterial could be used in a therapeutic dose to reduce the effects on cells with normal TfR levels.

Endocytosis of the nanoshells was best seen using confocal microscopy. The images shown in Fig. 3 establish that some particles are taken within the cell by endocytosis as well as adhering to the cell surface. This is most clearly seen in the three confocal slices of the cells incubated with the Fe(III)-doped, silica nanoshells (Fig. 3, bottom panels). Red/orange spots can be seen in a similar position in all three frames indicating that the Fe(III)-doped, silica nanoshells are within the cell. Corresponding images for the cells treated with the plain silica nanoshells show almost no detectable uptake.

Transferrin receptor (TfR) blocking experiment

The targeting mechanism of the Fe(III)-doped, silica nanoshells was investigated by competitively blocking the transferrin receptors on the MDA-MB-231 cells with varying concentrations of added bovine holo-transferrin. Bovine holo-transferrin was used because the mammalian cell culture media is enriched

Table 1 Fluorescence ratio analysis for the adhesion/endocytosis of 100 nm plain and Fe-doped, SiO_2 nanoshells by MDA-MB-231 cells

	# of outlines	Fluorescence ratio (a.u.)	Fluorescence increase relative to control (%)
Cells only (control)	156	0.14 ± 0.03	N/A
50 μg SiO_2	100	0.16 ± 0.06	14
50 μg Fe-doped, SiO_2	107	0.20 ± 0.06	43
100 μg SiO_2	143	0.17 ± 0.09	21
100 μg Fe-doped, SiO_2	113	0.26 ± 0.22	86
200 μg SiO_2	116	0.22 ± 0.12	57
200 μg Fe-doped, SiO_2	117	0.23 ± 0.12	64

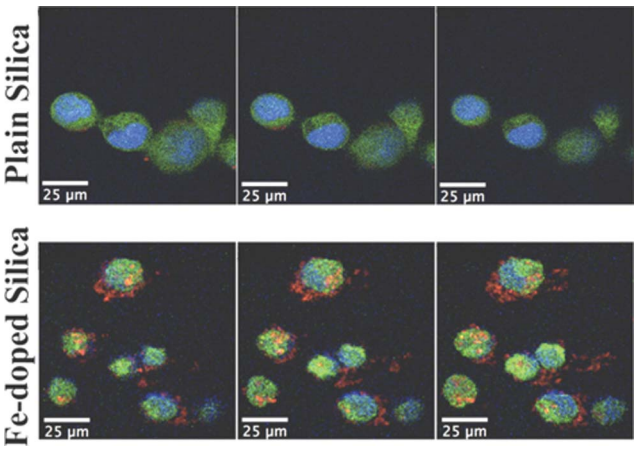

Fig. 3 Confocal microscopy images of 100 nm plain silica (top) and Fe(III)-doped silica (lower panels) nanoshell uptake by MDA-MB-231 cells. The images shown are for three successive slices of the cell separated by 1 micron within the cells. The top row images are for cells incubated with the plain silica nanoshells at 100 ug mL^{-1}. The Fe(III)-doped, silica nanoshells (bottom, also 100 ug mL^{-1}) can be seen in similar positions in all three images indicating the nanoshells are within the cell. All scale bars in the images are 25 microns.

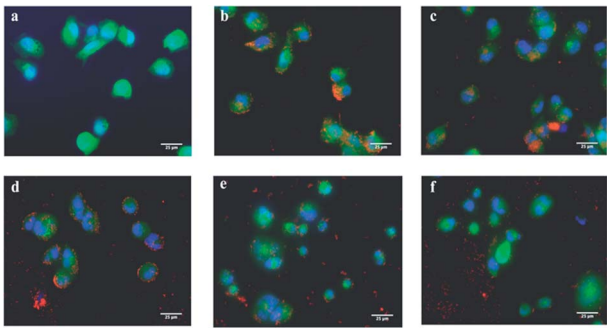

Fig. 4 Fluorescence microscopy images of bovine holoTf blocking experiment. Panel (a) control with 0 μM holoTf and no nanoshells added to the cells. The subsequent images show the amount of 100 nm Fe(III)-doped, silica nanoshells taken up by MDA-MB-231 cells when cells were pre-incubated for 2 hours with increasing amounts of holoTf: (b) 0 μM holoTf; (c) 20 μM holoTf; (d) 200 μM holoTf; (e) 500 μM holoTf; and (f) 1000 μM holoTf. After the pre-incubation step, cells were incubated with 50 μg mL^{-1} of AlexaFluor 680 coated, 100 nm Fe(III)-doped, silica nanoshells. All scale bars in the images are 25 microns.

with fetal bovine serum. Thus, the cells are acclimated to bovine transferrin. MDA-MB-231 cells were plated, in duplicate, as performed in the adhesion/endocytosis experiment. The cells were then allowed to incubate with 0, 20, 200, 500, or 1000 μM holo-transferrin for 2 h before addition of AlexaFluor 680 labeled, 100 nm Fe(III)-doped, silica nanoshells. Once the nanoshells were added to the cells, they were incubated for 24 h. The slides were then prepared for imaging as detailed in the methods section for the adhesion/endocytosis experiment.

The results of the blocking experiment can be seen in Fig. 4. As the concentration of holo-transferrin was increased from 0 μM (frame b) to 1000 μM (frame f) it was observed that the uptake of Fe(III)-doped, nanoshells by the MDA-MB-231 cells decreased. When the cells were incubated with 200 μM holo-transferrin, it appears that while some Fe(III)-doped, silica nanoshells accumulate on the surface of the cell, they do not undergo transport into the cell. Reduced nanoparticle uptake due to TfR blocking has also been observed for transferrin-labeled, gold nanoparticles.[77]

Fluorescence ratio analysis was also performed on the microscopy images recorded for the blocking experiment. Table 2 shows that the number of Fe-doped, SiO_2 nanoshells taken into the cells was significantly reduced on competitive blocking of the transferrin receptor. The uptake of Fe(III)-doped, SiO_2 nanoshells appears to be the same for the cells that were not blocked and the cells incubated with 20 μM holoTf. This indicates that 20 μM holoTf is not a high enough concentration to competitively block a significant number of Tf receptors. The addition of 200 μM holoTf shows a slight, but not statistically significant, decrease in fluorescence intensity relative to the control. A more significant decrease is observed with the addition of 500 μM and 1000 μM holoTf, which show effective blocking of Fe(III)-doped, SiO_2 nanoshell uptake by the TfR-mediated pathway. Fluorescence ratio analysis on the cell outlines was at the border of statistical significance (Table 2), so an alternative approach was used to better quantify blocking.

Fluorescence-activated cell sorting (FACS) was performed to study the effect of nanoshell uptake on blocking the transferrin receptor. MDA-MB-231 cells were pipetted into a standard 96-well plate and incubated with the same concentrations of holo-transferrin used to obtain the fluorescence microscopy images (0, 20, 200, 500, and 1000 μM). Since MDA-MB-231 is an adherent cell line, the cells were agitated every 20 min during incubation. AlexaFluor 488-labeled, Fe(III)-doped, silica

Table 2 Fluorescence ratio analysis for blocking experiment. All samples had 50 μg mL^{-1} of AlexaFluor 680 coated, 100 nm Fe(III)-doped, silica nanoshells added unless noted otherwise

	# of outlines	Fluorescence ratio (a.u.)	Fluorescence increase relative to control (%)
Cells only (no nano-shells)	82	0.10 ± 0.04	N/A
0 μM holoTf (no blocking)	75	0.31 ± 0.14	210
20 μM holoTf	84	0.35 ± 0.16	250
200 μM holoTf	84	0.26 ± 0.09	160
500 μM holoTf	101	0.16 ± 0.07	60
1000 μM holoTf	67	0.17 ± 0.07	70

nanoshells were added to the cells and the cells were incubated for another 3 h with agitation of the cells in 20 min intervals.

The results obtained using FACS, seen in Fig. 5, confirm that blocking of the transferrin receptor reduces the uptake of the Fe(III)-doped, silica nanoshells. Panel a of Fig. 5 shows the distribution of cell fluorescence for cells only (red), AlexaFluor 488-labeled nanoshells only (green), cells with nanoshells only (orange), and cells + 1000 μM holo-transferrin + nanoshells (blue). When the cells are treated with 1000 μM holo-transferrin there is a noticeable shift in their fluorescence properties toward that of untreated cells, as evidenced by the shift of the curve to the left relative to the curve with no added holo-Tf. The inhibition was not complete (cells only curve) as some Fe(III)-doped, silica nanoshells still underwent endocytosis or were adhering to the cells. Some non-receptor mediated nanoshell uptake can arise due to the small size of the nanoshells, as previously discussed.

Panel b in Fig. 5 is an overlay of the histograms obtained by varying concentrations of holo-transferrin used to treat the cells. A significant decrease in nanoshell uptake is not apparent until the cells were treated with 500 μM holo-transferrin. This agrees with the fluorescence microscopy observations in Fig. 4 and the luminescence ratio analysis (Table 2). Recall that with 200 μM holo-transferrin (Fig. 4), frame (d) added, the nanoshells appear to only adhere to the surface of the cell. This also agrees with the FACS experiment as the histogram obtained for the cells treated with 200 μM holo-transferrin completely overlies the histogram of the cells treated with nanoshells and no holo-transferrin. Zheng *et al.* have previously used FACS to successfully monitor the uptake of Tf-modified PLGA nanoparticles in SKBR-3 breast cancer cells.[78]

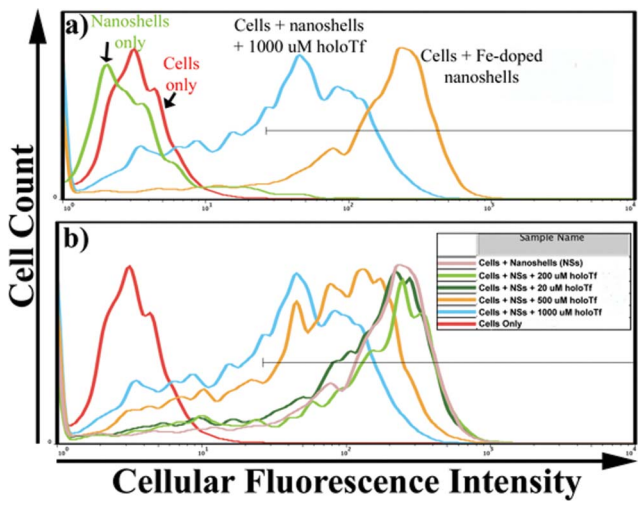

Fig. 5 Histograms obtained from FACS analysis of TfR blocking experiment. Panel a is a simplified version of the figure seen in panel b. The shift of the curve toward lower fluorescence intensity with added holo-Tf in panel a is the result of decreased nanoshell uptake by the MDA-MB-231 cells due to blocking of the TfR by holoTf. The histograms seen in panel b show that at least 500 μM holoTf needs to be added to the cells before a significant inhibition in nanoshell uptake could be observed.

Our previous work investigating the biodegradation of the Fe(III)-doped, silica nanoshells proposed that serum transferrin was binding to the iron(III) sites exposed on the surface in order to extract iron(III) and degrade the nanoparticle. The increased uptake of Fe(III)-doped, silica nanoshells observed in Fig. 2 and 3, and inhibition by blocking the TfR as seen in Fig. 4 and 5, appear to support the notion that transferrin attaches to the surface of the nanoshells. The decreased uptake observed in Fig. 4 and 5 after the addition of increasing concentrations of holoTf is consistent with Fe(III)-doped, silica nanoshells being taken into the cell *via* a transferrin receptor mediated pathway. Since transferrin was not added in the cell uptake/adhesion studies, the transferrin bound to the nanoshells must be endogenous Tf naturally found in the serum used to culture human cells. Since this transferrin was not covalently grafted to the nanoshell before its introduction into the biological media, it may offer a more robust form of targeting.

The targeting ability of nanoparticles with covalently grafted transferrin moieties can be neutralized due to lack of TfR recognition with the grafted transferrin or competition with free Tf.[79] Incompatibility may be minimized with the use of the Fe(III)-doped, silica nanoshells, because the transferrin that binds to the surface comes from an active source pool of Tf used in culturing the cells. Competition with free Tf may also be reduced by the sizeable fraction bound with the nanoshell dose. It is also possible that surface Fe(III) bound Tf presents a better conformation for TfR binding than covalently grafted Tf targeting approaches. The potential self-renewing process accompanying iron(III) removal, whereby new Tf molecules are expected to attack the nanoparticle surface as surface Fe(III) complexed Tf releases, may help renew targeting. The protein corona that coats targeted nanoparticles after they reside in complex biological media has been shown to reduce targeting effectiveness.[79] Further studies must be conducted to determine the level of targeting achieved *in vivo* by Fe(III) doped nanoparticles.

Conclusions

Fluorescence microscopy, in conjunction with confocal microscopy and FACS analysis, has shown that the doping of iron(III) into the silica matrix of a nanoshell imparts the nanoshell with a self-assembled targeting property for the transferrin receptor in the presence of endogenous serum transferrin. The iron(III)-doped, silica nanoshells do not require prior *in vitro* conjugation of the targeting ligand (transferrin) to its surface, which reduces the cost and complexity in the fabrication of targeted silica nanoparticles prepared by sol–gel methods. In addition, the iron(III) doping has already been shown to impart serum biodegradability to silica nanoparticles.[62] It is likely that surface iron(III) in an oxide nanoparticle may more generally enhance targeted nanoparticle endocytosis by the TfR mediated pathway, which could have broader significance. Silica and iron(III) doped nanoshells have shown promise for *in vitro* and *in vivo* ultrasound imaging agents.[76,80–83] A self-targeting property would potentially broaden their use to drug delivery and tumor localization.

Iron oxide nanoparticles used for MRI imaging have also been observed to undergo enhanced cellular uptake,[84–89] and a similar TfR mediated mechanism may be operative. It has also been observed that toxic heavy metals in aquatic environments adsorb to hydrated ferric oxide,[90,91] and this behavior is viewed as a potential method for removing toxic metals from the environment.[92–98] In the context of surface iron(III) providing a mechanism for endocytosis, the TfR mediated uptake of ferric oxide nanoparticles may need to be considered in assessing the bioavailability of heavy metals adsorbed on such iron oxide particles.

Abbreviations

APTES	3-Aminopropyltriethoxysilane
CMFDA	Chloromethylfluorescein diacetate
DMEM	Dulbecco's modified Eagle's medium
DPBS	Dulbecco's phosphate buffered saline
FACS	Fluorescence activated cell sorting
FBS	Fetal bovine serum
NS	Nanoshells
Tf	Transferrin
TfR	Transferrin receptor
holoTf	Holo-transferrin

Acknowledgements

This research was supported by the NIH Nanotumor Grant (NIH Grant no. U54 CA 119335) and the National Institute of Environmental Health Sciences (Award no. P42ES010337). In addition, individual student funding was provided by NCI Research Supplements to Promote Diversity in Health Related Research (NIH Grant no. 3U54 CA 119335-05S3), NSF—California LSAMP Bridge to the Doctorate/Louis Stokes Alliances for Minority Participation Fellowship (UCINSF Grant no. HRD0115115), and NIH—ET CURE/Specialized Cancer Center Support (Grant no. 3P30 CA 023100–25S7). We would like to acknowledge the UCSD Cancer Center Specialized Support Grant P30 CA23100 for assistance with obtaining the confocal images. K.K.P.M. thanks the UCSD Socrates Program for providing an NSF GK-12 STEM fellowship.

References

1 E. Gianotti, C. A. Bertolino, C. Benzi, G. Nicotra, G. Caputo, R. Castino, C. Isidoro and S. Coluccia, *ACS Appl. Mater. Interfaces*, 2009, **1**, 678–687.
2 E. Herz, A. Burns, S. Lee, P. Sengupta, D. Bonner, H. Ow, C. Liddell, B. Baird and U. Wiesner, *Proc. SPIE-Int. Soc. Opt. Eng.*, 2006, **6096**, 609605.
3 T. Hiroki, S. Taira, H. Katayanagi, Y. Moro, D. Shigeoka, S. Kimura, T. Mashino and Y. Ichiyanagi, *J. Phys.: Conf. Ser.*, 2010, **200**, 1–5.
4 C.-H. Lee, S.-H. Cheng, Y.-J. Wang, Y.-C. Chen, N.-T. Chen, J. Souris, C.-T. Chen, C.-Y. Mou, C.-S. Yang and L.-W. Lo, *Adv. Funct. Mater.*, 2009, **19**, 215–222.
5 W. C. Trogler, S. C. Esener, D. Messmer, J. U. Lind, K. Pohaku and J. Yang, *US Pat.* No. 20130230570, US, 2013, p. 76.
6 S. Sandoval, J. Yang, J. G. Alfaro, A. Liberman, M. Makale, C. E. Chiang, I. K. Schuller, A. C. Kummel and W. C. Trogler, *Chem. Mater.*, 2012, **24**, 4222–4230.
7 A. Liberman, N. Mendez, W. C. Trogler and A. C. Kummel, *Surf. Sci. Rep.*, 2014, **69**, 132–158.
8 I. Ortac, D. Simberg, Y.-s. Yeh, J. Yang, B. Messmer, W. C. Trogler, R. Y. Tsien and S. Esener, *Nano Lett.*, 2014, **14**, 3023–3032.
9 K. E. Uhrich, S. M. Cannizzaro, R. S. Langer and K. M. Shakesheff, *Chem. Rev.*, 1999, **99**, 3181–3198.
10 R. H. Fang, C.-M. J. Hu, B. T. Luk, W. Gao, J. A. Copp, Y. Tai, D. E. O'Connor and L. Zhang, *Nano Lett.*, 2014, **14**, 2181–2188.
11 C.-M. J. Hu, R. H. Fang, B. T. Luk and L. Zhang, *Nanoscale*, 2014, **6**, 65–75.
12 M. Sethi, R. Sukumar, S. Karve, M. E. Werner, E. C. Wang, D. T. Moore, S. R. Kowalczyk, L. Zhang and A. Z. Wang, *Nanoscale*, 2014, **6**, 2321–2327.
13 J. D. Byrne, T. Betancourt and L. Brannon-Peppas, *Adv. Drug Delivery Rev.*, 2008, **60**, 1615–1626.
14 M. M. Galagudza, D. V. Korolev, D. L. Sonin, V. N. Postnov, G. V. Papayan, I. S. Uskov, A. V. Belozertseva and E. V. Shlyakhto, *Int. J. Nanomed.*, 2010, **5**, 231–237.
15 V. Soni, S. K. Jain and D. V. Kohli, *Am. J. Drug Delivery*, 2005, **3**, 155–170.
16 W. P. Faulk, H. Harats, J. A. McIntyre, A. Berczi, I. L. Sun and F. L. Crane, *Am. J. Reprod. Immunol.*, 1989, **21**, 151–154.
17 F. X. Gu, R. Karnik, A. Z. Wang, F. Alexis, E. Levy-Nissenbaum, S. Hong, R. S. Langer and O. C. Farokhzad, *Nano Today*, 2007, **2**, 14–21.
18 B. Moulari, D. Pertuit, Y. Pellequer and A. Lamprecht, *Biomaterials*, 2008, **29**, 4554–4560.
19 C.-L. Zhu, X.-Y. Song, W.-H. Zhou, H.-H. Yang, Y.-H. Wen and X.-R. Wang, *J. Mater. Chem.*, 2009, **19**, 7765–7770.
20 A. Garcia-Bennett, M. Nees and B. Fadeel, *Biochem. Pharmacol.*, 2011, **81**, 976–984.
21 V. Saxena, Y. Naguib and M. D. Hussain, *Colloids Surf., B*, 2012, **94**, 274–280.
22 M. E. Werner, S. Karve, R. Sukumar, N. D. Cummings, J. A. Copp, R. C. Chen, T. Zhang and A. Z. Wang, *Biomaterials*, 2011, **32**, 8548–8554.
23 E. Werner Michael, S. Karve, R. Sukumar, D. Cummings Natalie, A. Copp Jonathan, C. Chen Ronald, T. Zhang and Z. Wang Andrew, *Biomaterials*, 2011, **32**, 8548–8554.
24 N. L. Adolphi, K. S. Butler, D. M. Lovato, T. E. Tessier, J. E. Trujillo, H. J. Hathaway, D. L. Fegan, T. C. Monson, T. E. Stevens, D. L. Huber, J. Ramu, M. L. Milne, S. A. Altobelli, H. C. Bryant, R. S. Larson and E. R. Flynn, *Contrast Media Mol. Imaging*, 2012, **7**, 308–319.
25 P. Debbage, *Curr. Pharm. Des.*, 2009, **15**, 153–172.
26 F. Fay and C. J. Scott, *Immunotherapy*, 2011, **3**, 381–394.
27 N. K. Mehra, V. Mishra and N. K. Jain, *Ther. Delivery*, 2013, **4**, 369–394.
28 H. K. Sajja, M. P. East, H. Mao, Y. A. Wang, S. Nie and L. Yang, *Curr. Drug Discovery Technol.*, 2009, **6**, 43–51.

29 S. Mansouri, Y. Cuie, F. Winnik, Q. Shi, P. Lavigne, M. Benderdour, E. Beaumont and J. C. Fernandes, *Biomaterials*, 2006, **27**, 2060–2065.
30 G. Zhai, J. Wu, B. Yu, C. Guo, X. Yang and R. J. Lee, *J. Nanosci. Nanotechnol.*, 2010, **10**, 5129–5136.
31 S. Das, S. Mitra, S. M. P. Khurana and N. Debnath, *Front. Life Sci.*, 2013, **7**, 90–98.
32 K. Park, *ACS Nano*, 2013, **7**, 7442–7447.
33 L. Zhang, Y. Li and J. C. Yu, *J. Mater. Chem. B*, 2014, **2**, 452–470.
34 T. R. Daniels, T. Delgado, J. A. Rodriguez, G. Helguera and M. L. Penichet, *Clin. Immunol.*, 2006, **121**, 144–158.
35 J. Fahrmeir and M. Ogris, in *Delivery of Protein and Peptide Drugs in Cancer*, ed. V. P. Torchilin, Imperial College Press, London, 2006, pp. 205–223.
36 Y. Jiang, G. Tang, M. Hong, S. Zhu, C. Fang, B. Shi and Y. Pei, *J. Drug Targeting*, 2007, **15**, 672–683.
37 H. Li, H. Sun and Z. M. Qian, *Trends Pharmacol. Sci.*, 2002, **23**, 206–209.
38 L. S. Mendonca, F. Firmino, J. N. Moreira, d. L. M. C. Pedroso and S. Simoes, *Bioconjugate Chem.*, 2010, **21**, 157–168.
39 Z. M. Qian, H. Li, H. Sun and K. Ho, *Pharmacol. Rev.*, 2002, **54**, 561–587.
40 Q. Xia, X.-W. Yang, X.-D. Yang, Z.-M. Qian and K. Wang, *J. Chin. Pharm. Sci.*, 2009, **18**, 7–13.
41 Y. Huang, L. He, W. Liu, C. Fan, W. Zheng, Y. S. Wong and T. Chen, *Biomaterials*, 2013, **34**, 7106–7116.
42 E. R. Camp, C. Wang, E. C. Little, P. M. Watson, K. F. Pirollo, A. Rait, D. J. Cole, E. H. Chang and D. K. Watson, *Cancer Gene Ther.*, 2013, **20**, 222–228.
43 W. Du, Y. Fan, N. Zheng, B. He, L. Yuan, H. Zhang, X. Wang, J. Wang, X. Zhang and Q. Zhang, *Biomaterials*, 2013, **34**, 794–806.
44 Y. Huang, L. He, W. Liu, C. Fan, W. Zheng, Y.-S. Wong and T. Chen, *Biomaterials*, 2013, **34**, 7106–7116.
45 P. Youn, Y. Chen and D. Y. Furgeson, *Mol. Pharmaceutics*, 2014, **11**, 486–495.
46 I. Bertini, H. B. Gray, E. I. Stiefel and J. S. Valentine, *Biological Inorganic Chemistry: Structure and Reactivity*, University Science Books, Sausalito, CA, 2007.
47 K. Thorstensen and I. Romslo, *Scand. J. Clin. Lab. Invest., Suppl.*, 1993, **215**, 113–120.
48 K. A. D. Sai, R. K. Mandraju, G. Kishore and A. K. Kondapi, *PLoS One*, 2009, **4**, 1–13.
49 F. Foda Mohamed, L. Huang, F. Shao and H.-Y. Han, *ACS Appl. Mater. Interfaces*, 2014, **6**, 2011–2017.
50 L.-C. Wu, L.-W. Chu, L.-W. Lo, Y.-C. Liao, Y.-C. Wang and C.-S. Yang, *ACS Nano*, 2013, **7**, 365–375.
51 M. Al Robaian, K. Y. Chiam, D. R. Blatchford and C. Dufes, *Nanomedicine*, 2014, **9**, 421–434.
52 H. C. Arora, M. P. Jensen, Y. Yuan, A. Wu, S. Vogt, T. Paunesku and G. E. Woloschak, *Cancer Res.*, 2012, **72**, 769–778.
53 S. S. Banerjee, D. Paul, S. G. Bhansali, N. D. Aher, A. Jalota-Badhwar and J. Khandare, *Small*, 2012, **8**, 1657–1663.
54 U.-J. Choe, A. R. Rodriguez, B. S. Lee, S. M. Knowles, A. M. Wu, T. J. Deming and D. T. Kamei, *Biomacromolecules*, 2013, **14**, 1458–1464.
55 Y. M. Li, D. A. Vallera and W. A. Hall, *J Neuro-Oncol.*, 2013, **114**, 155–164.
56 R. R. Sawant, A. M. Jhaveri, A. Koshkaryev, L. Zhu, F. Qureshi and V. P. Torchilin, *Mol. Pharmaceutics*, 2014, **11**, 375–381.
57 C. Tros de Ilarduya and N. Duezguenes, *Expert Opin. Drug Delivery*, 2013, **10**, 1583–1591.
58 Y. Yang, X. Zhang, X. Wang, X. Zhao, T. Ren, F. Wang and B. Yu, *Int. J. Pharm.*, 2014, **467**, 113–122.
59 J. Yue, S. Liu, R. Wang, X. Hu, Z. Xie, Y. Huang and X. Jing, *Mol. Pharmaceutics*, 2012, **9**, 1919–1931.
60 F. Dilnawaz, A. Singh and S. K. Sahoo, *Acta Biomater.*, 2012, **8**, 704–719.
61 M. Kresse, S. Wagner, D. Pfefferer, R. Lawaczeck, V. Elste and W. Semmler, *Magn. Reson. Med.*, 1998, **40**, 236–242.
62 K. K. P. Mitchell, A. Liberman, A. C. Kummel and W. C. Trogler, *J. Am. Chem. Soc.*, 2012, **134**, 13997–14003.
63 A. Butler, *Nat. Struct. Biol.*, 2003, **10**, 240–241.
64 S. M. Kraemer, A. Butler, P. Borer and J. Cervini-Silva, *Rev. Mineral. Geochem.*, 2005, **59**, 53–84.
65 K. N. Raymond and B. L. Bryan, *NATO ASI Ser., Ser. C*, 1995, 13–24.
66 A. Butler and R. M. Theisen, *Coord. Chem. Rev.*, 2010, **254**, 288–296.
67 A. Calzolari, I. Oliviero, S. Deaglio, G. Mariani, M. Biffoni, N. M. Sposi, F. Malavasi, C. Peschle and U. Testa, *Blood Cells, Mol., Dis.*, 2007, **39**, 82–91.
68 T. Inoue, P. G. Cavanaugh, P. A. Steck, N. Brunner and G. L. Nicolson, *J. Cell. Physiol.*, 1993, **156**, 212–217.
69 M. B. Omary, I. S. Trowbridge and J. Minowada, *Nature*, 1980, **286**, 888–891.
70 J. Yang, S. Sandoval, J. G. Alfaro, S. Aschemeyer, A. Liberman, D. T. Martin, M. Makale, A. C. Kummel and W. C. Trogler, *J. Biomed. Opt.*, 2011, **16**, 066012.
71 J. Yang, J. U. Lind and W. C. Trogler, *Chem. Mater.*, 2008, **20**, 2875–2877.
72 M. P. Desai, V. Labhasetwar, E. Walter, R. J. Levy and G. L. Amidon, *Pharm. Res.*, 1997, **14**, 1568–1573.
73 S. Prabha, W.-Z. Zhou, J. Panyam and V. Labhasetwar, *Int. J. Pharm.*, 2002, **244**, 105–115.
74 I. Slowing, B. G. Trewyn and V. S. Y. Lin, *J. Am. Chem. Soc.*, 2006, **128**, 14792–14793.
75 I. I. Slowing, J. L. Vivero-Escoto, Y. Zhao, K. Kandel, C. Peeraphatdit, B. G. Trewyn and V. S. Y. Lin, *Small*, 2011, **7**, 1526–1532.
76 A. Liberman, Z. Wu, C. V. Barback, R. Viveros, S. L. Blair, L. G. Ellies, D. R. Vera, R. F. Mattrey, A. C. Kummel and W. C. Trogler, *ACS Nano*, 2013, **7**, 6367–6377.
77 P.-H. Yang, X. Sun, J.-F. Chiu, H. Sun and Q.-Y. He, *Bioconjugate Chem.*, 2005, **16**, 494–496.
78 Y. Zheng, B. Yu, W. Weecharangsan, L. Piao, M. Darby, Y. Mao, R. Koynova, X. Yang, H. Li, S. Xu, L. J. Lee, Y. Sugimoto, R. W. Brueggemeier and R. J. Lee, *Int. J. Pharm.*, 2010, **390**, 234–241.
79 A. Salvati, A. S. Pitek, M. P. Monopoli, K. Prapainop, F. B. Bombelli, D. R. Hristov, P. M. Kelly, C. Aberg, E. Mahon and K. A. Dawson, *Nat. Nanotechnol.*, 2013, **8**, 137–143.

80 A. Liberman, H. P. Martinez, C. N. Ta, C. V. Barback, R. F. Mattrey, Y. Kono, S. L. Blair, W. C. Trogler, A. C. Kummel and Z. Wu, *Biomaterials*, 2012, **33**, 5124–5129.
81 H. P. Martinez, Y. Kono, S. L. Blair, S. Sandoval, J. Wang-Rodriguez, R. F. Mattrey, A. C. Kummel and W. C. Trogler, *MedChemComm*, 2010, **1**, 266–270.
82 C. N. Ta, A. Liberman, H. Paul Martinez, C. V. Barback, R. F. Mattrey, S. L. Blair, W. C. Trogler, A. C. Kummel and Z. Wu, *J. Vac. Sci. Technol., B: Nanotechnol. Microelectron.: Mater., Process., Meas., Phenom.*, 2012, **30**, 02C104.
83 A. Liberman, Z. Wu, C. V. Barback, R. D. Viveros, J. Wang, L. G. Ellies, R. F. Mattrey, W. C. Trogler, A. C. Kummel and S. L. Blair, *J. Surg. Res.*, 2014, **190**, 391–398.
84 W.-H. Chiang, W.-C. Huang, C.-W. Chang, M.-Y. Shen, Z.-F. Shih, Y.-F. Huang, S.-C. Lin and H.-C. Chiu, *J. Controlled Release*, 2013, **168**, 280–288.
85 M. Krause, K. K. Kwong, J. Xiong, E. S. Gragoudas and L. H. Y. Young, *Ophthalmic Res.*, 2002, **34**, 241–250.
86 S. Laurent, S. Boutry, I. Mahieu, L. Vander Elst and R. N. Muller, *Curr. Med. Chem.*, 2009, **16**, 4712–4727.
87 E. Schulze, J. T. Ferrucci, Jr., K. Poss, L. Lapointe, A. Bogdanova and R. Weissleder, *Invest. Radiol.*, 1995, **30**, 604–610.
88 H. Bakhru Sasha, E. Altiok, C. Highley, D. Delubac, J. Suhan, T. K. Hitchens, C. Ho and S. Zappe, *Int. J. Nanomed.*, 2012, **7**, 4613–4623.
89 J. Huang, L. Bu, J. Xie, K. Chen, Z. Cheng, X. Li and X. Chen, *ACS Nano*, 2010, **4**, 7151–7160.
90 R. Aryal, S. Vigneswaran, P. Loganathan, J. Kandasamy and T. Mohammed, *Korean J. Chem. Eng.*, 2011, **28**, 1706–1712.
91 S. N. Luoma and J. A. Davis, *Mar. Chem.*, 1983, **12**, 159–181.
92 A. Z. M. Badruddoza, Z. B. Z. Shawon, W. J. D. Tay, K. Hidajat and M. S. Uddin, *Carbohydr. Polym.*, 2013, **91**, 322–332.
93 P. Bhunia, G. Kim, C. Baik and H. Lee, *Chem. Commun.*, 2012, **48**, 9888–9890.
94 J.-S. Hu, L.-S. Zhong, W.-G. Song and L.-J. Wan, *Adv. Mater.*, 2008, **20**, 2977–2982.
95 S. Mahdavi, M. Jalali and A. Afkhami, *J. Nanopart. Res.*, 2012, **14**, 846.
96 S. K. Maji, Y. H. Kao and C. W. Liu, *Desalination*, 2011, **280**, 72–79.
97 T. Phuengprasop, J. Sittiwong and F. Unob, *J. Hazard. Mater.*, 2011, **186**, 502–507.
98 B. S. Tawabini, S. F. Al-Khaldi, M. M. Khaled and M. A. Atieh, *J. Environ. Sci. Health, Part A: Toxic/Hazard. Subst. Environ. Eng.*, 2011, **46**, 215–223.